# Flight Effects on Noise from Coaxial Dual Flow Part I: Unheated Jets

R. Dash*
*NASA Ames Reserch Center, Moffett Field, California*

**This paper and a companion work describe a theoretical study of the effects of forward flight on the far-field noise radiated from coaxial jets. Cold jets are examined here and hot jets in Part II. The noise generation is modeled by two sets of embedded compact, ring sources that are uncorrelated, thereby allowing linear superposition to be used in the mathematical solution. The problem is further characterized as a double vortex-sheet model involving deliberate suppression of the inherent instabilities of the flow. The analysis shows that the effects of flight induce 1) amplification of noise in the forward quadrant, 2) reduction of noise in the aft quadrant, and 3) absolutely no effect on radiation of noise at $\theta = 90$ deg to the jet axis. It is also shown that at constant mass flow and thrust, an inverted velocity profile jet provides a significant noise reduction (as compared to noise from a conventional profile jet) at all angles, both statically and in flight.**

## Nomenclature

$c$ = speed of sound
$d$ = diameter of the inner nozzle
$D$ = diameter of the outer nozzle
$I$ = intensity of radiation
$k$ = wave number
$K$ = propagation constant
$M$ = Mach number of the jet flow
$\bar{M}$ = $U_m/c_0$
$M_c$ = Mach number of source convection in the primary flow, $U_c/c_0$
$\mathfrak{M}_c$ = Mach number of source convection in the secondary flow, $\mathfrak{U}_c/c_0$
$m$ = periodicity of the source in the primary flow
$n$ = periodicity of the source in the secondary flow
$p$ = acoustic pressure
$q_m$ = strength of the ring source in the primary flow
$q_n$ = strength of the ring source in the secondary flow
$r$ = axial distance in the radial direction
$r_p$ = radius of the primary flow
$r_s$ = radius of the secondary flow
$r_0$ = axial distance of the ring source in the primary flow
$\mathfrak{r}_0$ = axial distance of the ring source in the secondary flow
$R$ = distance between the source (in the primary flow) and the observer
$\mathfrak{R}$ = distance between the source (in the secondary flow) and the observer
$St_1$ = Strouhal number associated with source in the primary flow
$St_2$ = Strouhal number associated with source in the secondary flow
$U$ = velocity of the jet flow
$U_c$ = convection velocity of the source in the primary flow
$\mathfrak{U}_c$ = convection velocity of the source in the secondary flow
$U_m$ = characteristic mean velocity
$w$ = frequency of the source in the secondary flow
$\Gamma$ = $U_s/U_p$
$\theta$ = angle of emission relative to the jet axis (at the retarded time)
$\rho$ = density
$\Sigma$ = outer-to-inner area ratio
$\omega$ = frequency of the source in the primary flow

*Subscripts*

$f$ = conditions pertaining to flight
$p$ = conditions in the primary flow
$s$ = conditions in the secondary flow
$rcp$ = conditions due to a ring source in the cold primary flow
$rcs$ = conditions due to a ring source in the cold secondary flow
$rhp$ = conditions due to a ring source in the hot primary flow
$rhs$ = conditions due to a ring source in the hot secondary flow
0 = ambient conditions

## Introduction

IN the past few years, several studies suggest that a large-scale orderly structure lies hidden within the chaotic, noise-producing, transition region of a jet. Using several methods in their study of flow visualization of round jets, Crow and Champagne[1] discovered the emergence of an orderly flow pattern. They also noticed that, at an average Strouhal number of about 0.3 based on frequency, exit speed, and diameter, a tenuous train of puffs/rings having axisymmetric structure is generated in the transitional turbulence region of a jet. These rings are highly structured and stable. The production of doughnut-like rings also finds support in the works of Wooldridge and Wooten.[2] Hardin[3] used the ring sources to analyze the noise-producing potential of round jets and observed that these rings may be responsible for most of the jet noise. Crow and Champagne observed from their previous work on water jets "waves radiating outward from the above region of puff formation." These and several similar inferences of the research workers prompted the author to include the ring sources in the study of jet noise through the vortex sheet modeling of the flow.

The prediction model contains three major elements: 1) convection of acoustic sources in the primary and secondary flows, 2) flow/acoustic interaction due to these two constituent streams, and 3) the effects of flight. Furthermore, all possible combinations of unheated (Part I) and heated jets

Received Nov. 20, 1984; revision received Aug. 3, 1985. 

*NRC-NASA Senior Resident Research Associate; presently Senior Acoustics Engineer, Douglas Aircraft Company, Long Beach, CA. Member AIAA.

(Part II)[16] that comprise a coaxial dual flow have also been built into the model.

The motivation for this work comes from the recent advances in theoretical modeling of jet noise by Mani.[4,5] Mani's approach is one of the successful approaches to jet noise problems in recent years, despite its simplicity. He capitalized on a simplified form of a mathematically rigorous, nonlinear, inhomogeneous wave equation originated by Phillips[6] and developed more fully by Lilley,[7] and Goldstein and Howes.[8] Mani's model succeeds in explaining most major interesting features of jet noise data, on both hot and cold jets, not explainable by the Lighthill approach, especially the flow/acoustic interaction.

In general, many of the experimental features are consistent with the results of the vortex sheet flow model procedure, which deliberately suppresses the instability waves that actually show up in any physical realization being described by that model. Balsa and Gliebe[9] recognized this general feature of the vortex sheet flow model and the ease and straightforwardness with which it is handled and extended Mani's theory to explain the noise radiation from coaxial jets. In their work, however, they describe a static jet noise situation. Furthermore, by considering only a single point source at the centerline of a primary jet in a coaxial flow, they failed to provide a correct model since it did not represent all of the sources generated at the interface between the two vortices.

In recent works, Dash[10-12] extended the Mani-type vortex sheet flow model to include the effects of flight. Dash predicted the different features associated with the noise from a single stream jet in flight as well as from a coaxial jet in flight. However, the model proved to be inadequate, since only the acoustic sources due to the primary/secondary flow interactions were taken into consideration, while the acoustic sources due to the secondary/ambient flow interactions were inadvertently omitted.

In the present work, this omission was corrected by considering simultaneously the sources within the inner and outer jets. The first set of sources represent the noise from the interaction between the inner and outer flows. These sources are presumed to be axially and symmetrically distributed in and around the primary flow and as such can be qualitatively represented by considering a ring source convecting in the midst of the primary jet. The second set of sources represent the noise from the interaction between the outer and the ambient flows. The sources are also presumed to be axially and symmetrically distributed in and around the secondary flow. These sources are qualitatively represented by considering a ring source convecting in the midst of the secondary jet. The choice for the centerline convection is strongly advocated and also found to have been applied to yield very good results in the works of Mani.[4,5] This is also supported by the experimental evidence in the work of Scharton and his colleagues.[13] Furthermore, Mani[14] has also argued that the exact location of the source does not matter so long as it is well within the jet. These ideas help significantly in the handling of mathematics involved in the analysis.

## Formulation and Mathematical Development of the Model

The analysis is intended to model the situation shown in Fig. 1, in which a coflowing coaxial dual jet exhausts into the atmosphere from a nozzle. The flight simulation of the model is shown in Fig. 2. The nozzle is moving in an opposite direction with velocity $U_f$, which is the velocity of flight. The inner stream of radius $r_p$, called the primary stream, is characterized by velocity $U_p$ and the outer stream of radius $r_s$, called the secondary stream, is characterized by velocity $U_s$. Likewise, all the flow parameters (density $\rho$, speed of sound $c$, Mach number $M$, etc.) associated with the inner/primary flow are designated by the subscript $p$ and those with the outer/secondary flow are designated by the subscript $s$. As indicated earlier, two ring sources are introduced in the forms

Ring in the primary flow:

$$q_m \frac{\delta(r-r_0)}{r}\delta(z-U_c t)e^{i(m\phi-\omega t)}, \qquad 0<r_0<r_p \tag{1a}$$

Ring in the secondary flow:

$$q_n \frac{\delta(r-\mathfrak{r}_0)}{r}\delta(z-\mathfrak{U}_c t)e^{i(n\phi-wt)}, \qquad r_p<\mathfrak{r}_0<r_s \tag{1b}$$

where $q_m$ and $q_n$ are constants and reflect the characteristic ring strengths to which we will give proper meaning in due course. The quantities $\omega$ and $w$ are the frequencies associated with the ring sources in the primary and secondary flows and are directly related to the frequency with which the puffs are found. $U_c$ and $\mathfrak{U}_c$ are their respective velocities with which they convect. The propagation of waves in the fluids in different zones is governed by

$$\frac{1}{c_p^2}\left(\frac{\partial}{\partial t}+U_p\frac{\partial}{\partial z}\right)^2 p-\nabla^2 p = q_m L_j\left[\frac{\delta(r-r_0)}{r}\delta(z-U_c t)e^{i(m\phi-\omega t)}\right], \qquad 0\le r\le r_p \tag{2a}$$

$$\frac{1}{c_s^2}\left(\frac{\partial}{\partial t}+U_s\frac{\partial}{\partial z}\right)^2 p-\nabla^2 p = q_n \mathfrak{L}_j\left[\frac{\delta(r-\mathfrak{r}_0)}{r}\delta(z-\mathfrak{U}_c t)e^{i(n\phi-wt)}\right], \qquad r_p\le r\le r_s \tag{2b}$$

$$\frac{1}{c_f^2}\left(\frac{\partial}{\partial t}+U_f\frac{\partial}{\partial z}\right)^2 p-\nabla^2 p=0, \qquad r\ge r_s \tag{2c}$$

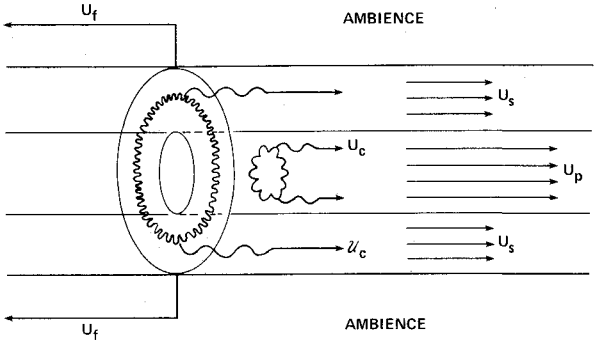


**Fig. 1 Practical configuration of the model.**

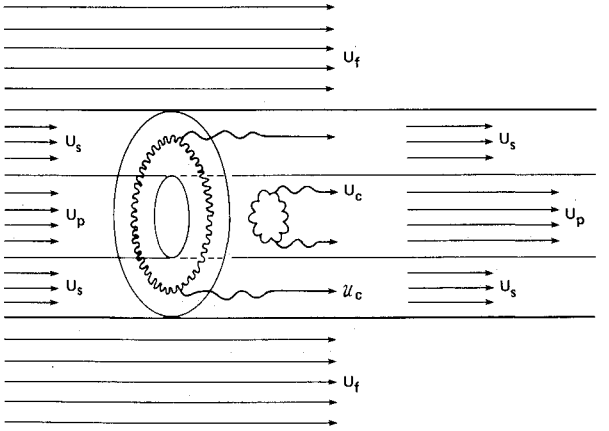


**Fig. 2 Flight simulation of the model.**

where the differential operators $L_j$ and $\mathfrak{L}_j$ are given by

$$L_1=\mathfrak{L}_1=1 \qquad L_3=\mathfrak{L}_3=\frac{\partial}{\partial z}$$

$$L_2=\frac{\partial}{\partial t}+U_p\frac{\partial}{\partial z}, \quad \mathfrak{L}_2=\frac{\partial}{\partial t}+U_s\frac{\partial}{\partial z}, \quad L_4=\mathfrak{L}_4=\frac{\partial^2}{\partial z^2} \tag{3}$$

The suffix $j$ takes the values $j=1,2,3,4$ corresponding to order of the acoustic pole (i.e., pulsating, mass fluctuation, dipole, or quadrupole type).

Because of the linearity of the equations and the involved boundary conditions, the two solutions can be superimposed. In other words, the resulting radiation effect will be the linear combination of the fields radiated by the ring sources in both the primary and secondary flows.

### Ring Source in the Secondary Stream

Directing attention to the problem of a coaxial jet flow with a ring source convecting in the secondary flow, it can be seen that the mathematical problem involves solving

$$\left[\frac{1}{c_p^2}\left(\frac{\mathrm{D}}{\mathrm{D}t}\right)_p^2-\nabla^2\right]p=0, \qquad 0\le r\le r_p \tag{4a}$$

$$\left[\frac{1}{c_s^2}\left(\frac{\mathrm{D}}{\mathrm{D}t}\right)_s^2-\nabla^2\right]p$$

$$=q_n\mathfrak{L}_j\left[\frac{\delta(r-r_0)}{r}\delta(z-\mathfrak{U}_c t)e^{i(n\phi-wt)}\right], \quad r_p\le r\le r_s \tag{4b}$$

$$\left[\frac{1}{c_f^2}\left(\frac{\mathrm{D}}{\mathrm{D}t}\right)_f^2-\nabla^2\right]p=0, \qquad r_s\le r \tag{4c}$$

where

$$\left(\frac{\mathrm{D}}{\mathrm{D}t}\right)_p=\frac{\partial}{\partial t}+U_p\frac{\partial}{\partial z}, \qquad \left(\frac{\mathrm{D}}{\mathrm{D}t}\right)_s=\frac{\partial}{\partial t}+U_s\frac{\partial}{\partial z}$$

$$\left(\frac{\mathrm{D}}{\mathrm{D}t}\right)_f=\frac{\partial}{\partial t}+U_f\frac{\partial}{\partial z} \tag{4d}$$

The boundary conditions across the primary/secondary flow interface at $r=r_p$ and the secondary/outer (simulating) flow interface at $r=r_s$ are the continuity of acoustic pressure and the continuity of normal particle displacement.

Using the property of $\delta$-function, the right-hand side source term in Eq. (4b) is given by

$$q_n\mathfrak{L}_j\left\{\frac{\delta(r-r_0)}{2\pi r}\int_{-\infty}^{\infty}\exp i[(k_3z+n\phi)-(w+k_3\mathfrak{U}_c)t]\,\mathrm{d}k_3\right\} \tag{5}$$

This is the driving term in the whole problem and as such the $\phi$, $z$, $t$ dependence of all quantities in the Fourier transform formulation will be $\sim\exp i[(k_3z+n\phi)-(w+k_3\mathfrak{U}_c)t]$. This is due to the fact that on a linear theory a term proportional to $e^{ikx}$ in the forcing effect elicits responses proportional to $e^{ikx}$ everywhere in the system, whereby the corresponding values of the acoustic pressure, velocity, displacement, potential, or any other acoustic parameter are themselves proportional to $e^{ikx}$. In view of this, the Fourier transforms of the pressure and displacement terms are defined as

$$p(r,\phi,z,t)=\int_{-\infty}^{\infty}\tilde{p}(r,k_3)\exp i[(k_3z+n\phi)-(w+k_3\mathfrak{U}_c)t]\,\mathrm{d}k_3 \tag{6a}$$

$$\eta(r,\phi,z,t)=\int_{-\infty}^{\infty}\tilde{\eta}(r,k_3)\exp i[(k_3z+n\phi)-(w+k_3\mathfrak{U}_c t)]\,\mathrm{d}k_3 \tag{6b}$$

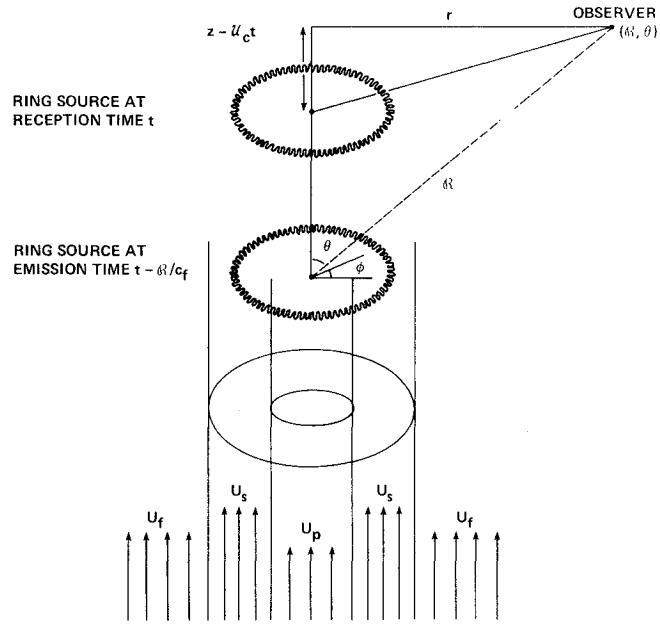


**Fig. 3 Retarded coordinates and emission from ring source in the secondary stream.**

Making use of these Fourier relations, the boundary conditions of continuity of normal particle displacement on $r=r_p$ and $r=r_s$, respectively, can be written as

$$\left(\frac{\rho_p}{\rho_s}\right)\left[\frac{k+(\mathfrak{M}_c-M_p)k_3}{k+(\mathfrak{M}_c-M_s)k_3}\right]^2\left(\frac{\partial\tilde{p}}{\partial r}\right)_{r_p(+)}=\left(\frac{\partial\tilde{p}}{\partial r}\right)_{r_p(-)} \tag{7a}$$

$$\left(\frac{\rho_s}{\rho_f}\right)\left[\frac{k+(\mathfrak{M}_c-M_s)k_3}{k+(\mathfrak{M}_c-M_f)k_3}\right]^2\left(\frac{\partial\tilde{p}}{\partial r}\right)_{r_s(+)}=\left(\frac{\partial\tilde{p}}{\partial r}\right)_{r_s(-)} \tag{7b}$$

Making use of the boundary conditions, a solution for the outgoing field can be written from the above equations as:

$$\tilde{p}(r,\mathcal{K}_f)=A_nH_n(\mathcal{K}_fr), \quad r_s\le r \tag{8a}$$

$$A_n=\frac{q_n}{2\pi r_s}\mathcal{K}_j(k_3)$$

$$\times\frac{J_n(\mathcal{K}_sr_0)\mathcal{G}_{sp}(Y_n,J_n)-Y_n(\mathcal{K}_sr_0)\mathcal{G}_{sp}(J_n,J_n)}{\mathcal{G}_{fs}(H_n,J_n)\mathcal{G}_{sp}(Y_n,J_n)-\mathcal{G}_{fs}(H_n,Y_n)\mathcal{G}_{sp}(J_n,J_n)} \tag{8b}$$

$$\mathcal{G}_{sp}(Y_n,J_n)=\mathcal{K}_s\mathcal{Q}_{ps}Y_n'(\mathcal{K}_sr_p)J_n(\mathcal{K}_pr_p)$$

$$-\mathcal{K}_pY_n(\mathcal{K}_sr_p)J_n'(\mathcal{K}_pr_p) \tag{8c}$$

$$\mathcal{G}_{sp}(J_n,J_n)=\mathcal{K}_s\mathcal{Q}_{ps}J_n'(\mathcal{K}_sr_p)J_n(\mathcal{K}_pr_p)$$

$$-\mathcal{K}_pJ_n(\mathcal{K}_sr_p)J_n'(\mathcal{K}_pr_p) \tag{8d}$$

$$\mathcal{G}_{fs}(H_n,J_n)=\mathcal{K}_f\mathcal{Q}_{sf}H_n'(\mathcal{K}_fr_s)J_n(\mathcal{K}_sr_s)$$

$$-\mathcal{K}_sH_n(\mathcal{K}_fr_s)J_n'(\mathcal{K}_sr_s) \tag{8e}$$

$$\mathcal{G}_{fs}(H_n,Y_n)=\mathcal{K}_f\mathcal{Q}_{sf}H_n'(\mathcal{K}_fr_s)Y_n(\mathcal{K}_sr_s)$$

$$-\mathcal{K}_sH_n(\mathcal{K}_fr_s)Y_n'(\mathcal{K}_sr_s) \tag{8f}$$

$$\mathcal{K}_p=(c_0/c_p)\{[k+(\mathfrak{M}_c-M_p)k_3]^2-k_3^2\}^{1/2} \tag{8g}$$

$$\mathcal{K}_s=(c_0/c_s)\{[k+(\mathfrak{M}_c-M_s)k_3]^2-k_3^2\}^{1/2} \tag{8h}$$

$$\mathcal{K}_f=(c_0/c_f)\{[k+(\mathfrak{M}_c-M_f)k_3]^2-k_3^2\}^{1/2} \tag{8i}$$

$$\mathcal{K}_1 = -1, \quad \mathcal{K}_2 = ic_0[k + (\mathfrak{M}_c - M_s)k_3] \tag{8j}$$

$$\mathcal{K}_2 = -ik_3, \quad \mathcal{K}_4 = k_3^2 \tag{8k}$$

where $J_n$ and $Y_n$ are Bessel functions of first and second kind of order $n$ and $H_n$ (same as $H_n^{(1)}$) the Hankel function of order $n$. Dashes denote differentiation with respect to the argument. This solution describes a wave radiating outward, subject to the condition $\mathcal{K}_f^2 \geq 0$, which yields

$$-k\left[\frac{c_f}{c_0} + (\mathfrak{M}_c - M_f)\right]^{-1} \leq k_3 \leq k\left[\frac{c_f}{c_0} - (\mathfrak{M}_c - M_f)\right]^{-1} \tag{9}$$

This inequality determines the range of $k_3$, which ensures a propagating-type solution of the radiation problem.

## Far-Field Low-Frequency Analysis

To express the acoustic pressure in Eq. (8) in Fourier space to a corresponding one in physical space, Eq. (6) is used to write

$$p(r,\phi,z,t) = \int_{-\infty}^{\infty} A_n H_n(\mathcal{K}_f r)\exp i[(k_3 z + n\phi) - (w + k_3 \mathfrak{U}_c)t]\,dk_3 \tag{10}$$

Evaluation of the above integral is prohibitively difficult because of the involved, complicated expression for $A_n$. Therefore, the method of stationary phase is used to find the far-field radiation which is of prime interest. Without going through the details of this method, the far-field expression for $p$ is given as

$$p(\mathfrak{R},\theta,\phi,t) = \frac{q_n}{i\pi r_s}\frac{\mathcal{K}_j(k_3)_0 E_n}{\mathfrak{R}} \times \frac{\exp i[\mathfrak{R}k(c_0/c_f) - wt + n(\phi - \pi/2)]}{[1-(c_0/c_f)(\mathfrak{M}_c - M_f)\cos\theta]} \tag{11a}$$

where $E_n$ and the stationary point $(k_3)_0$ are given by

$$E_n = \frac{J_n(\mathcal{K}_s r_0)\mathcal{G}_{sp}(Y_n,J_n) - Y_n(\mathcal{K}_s r_0)\mathcal{G}_{sp}(J_n,J_n)}{\mathcal{G}_{fs}(H_n,J_n)\mathcal{G}_{sp}(Y_n,J_n) - \mathcal{G}_{fs}(H_n,Y_n)\mathcal{G}_{sp}(J_n,J_n)} \tag{11b}$$

$$(k_3)_0 = \frac{k(c_0/c_f)\cos\theta}{1-(c_0/c_f)(\mathfrak{M}_c - M_f)\cos\theta} \tag{11c}$$

In view of this stationary point value,

$$\mathcal{K}_p = \frac{k}{1-(c_0/c_f)(\mathfrak{M}_c - M_f)\cos\theta}\left\{\left(\frac{c_0}{c_p}\right)^2 \times \left[1 - \frac{c_0}{c_f}(M_p - M_f)\cos\theta\right]^2 - \left(\frac{c_0}{c_f}\cos\theta\right)^2\right\}^{1/2} \tag{11d}$$

$$\mathcal{K}_s = \frac{k}{1-(c_0/c_f)(\mathfrak{M}_c - M_f)\cos\theta}\left\{\left(\frac{c_0}{c_s}\right)^2 \times \left[1 - \frac{c_0}{c_f}(M_s - M_f)\cos\theta\right]^2 - \left(\frac{c_0}{c_f}\cos\theta\right)^2\right\}^{1/2} \tag{11e}$$

$$\mathcal{K}_f = \frac{k(c_0/c_f)\sin\theta}{1-(c_0/c_f)(\mathfrak{M}_c - M_f)\cos\theta} \tag{11f}$$

$$\mathcal{K}_1 = -1, \quad \mathcal{K}_2 = ic_0 k\left[\frac{1-(c_0/c_f)(M_s - M_f)\cos\theta}{1-(c_0/c_f)(\mathfrak{M}_c - M_f)\cos\theta}\right] \tag{11g}$$

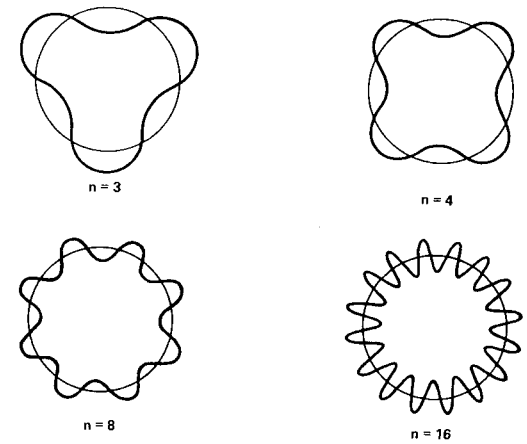


**Fig. 4 Periodicity of the ring source along $\phi$ (occurs in the form of $e^{in\phi}$).**

$$\mathcal{K}_3 = -ik\frac{c_0}{c_f}\frac{\cos\theta}{1-(c_0/c_f)(\mathfrak{M}_c - M_f)\cos\theta} \tag{11h}$$

$$\mathcal{K}_4 = \frac{(kc_0/c_f)^2\cos^2\theta}{[1-(c_0/c_f)(\mathfrak{M}_c - M_f)\cos\theta]^2} \tag{11i}$$

$$\mathfrak{A}_{ps} = \left(\frac{\rho_p}{\rho_s}\right)\left[\frac{1-(c_0/c_f)(M_p - M_f)\cos\theta}{1-(c_0/c_f)(M_s - M_f)\cos\theta}\right]^2 \tag{11j}$$

$$\mathfrak{A}_{sf} = \left(\frac{\rho_s}{\rho_f}\right)\left[1 - \frac{c_0}{c_f}(M_s - M_f)\cos\theta\right]^2 \tag{11k}$$

where $\mathfrak{R}$ and $\theta$ are shown in Fig. 3; these are the retarded coordinates.

In analyzing the low-frequency radiation of the pressure field, we make use of the limiting forms of Bessel and Hankel functions for small arguments so that a low-frequency far-field solution for the ring source in the secondary fluid is

$$p_n(\mathfrak{R},\theta,\phi,t) = -\frac{q_n \mathcal{K}_j(k_3)_0}{\Gamma(n+1)}\left(\frac{\mathcal{K}_f r_0}{2}\right)^n \times \left[\frac{(\mathfrak{A}_{ps}+1) + (\mathfrak{A}_{ps}-1)(r_p/r_0)^{2n}}{(\mathfrak{A}_{sf}+1)(\mathfrak{A}_{ps}+1) + (\mathfrak{A}_{sf}-1)(\mathfrak{A}_{ps}-1)(r_p/r_s)^{2n}}\right] \times \frac{\exp i[\mathfrak{R}k(c_0/c_f) - wt + n(\phi - \pi/2)]}{\mathfrak{R}[1-(c_0/c_f)(\mathfrak{M}_c - M_f)\cos\theta]} \tag{12}$$

The quantity $kr_0$ is implicit in $\mathcal{K}r_0$ and is itself a small quantity because of the low-frequency nature of the source. The use of the inequalities $r_p/r_0 < 1$ and $r_p/r_s <$ in the above yields

$$\underset{n\to\infty}{Lt}\left|\frac{p_{n+1}}{p_n}\right| \to 0 \tag{13}$$

where $p_n$ is the pressure due to the ring source having periodicity $n$ along $\phi$ that occurs in the form of $e^{in\phi}$. Thus, as shown above, one can infer that

$$|p_0| > |p_1| > |p_2| > \ldots > |p_n| > |p_{n+1}| > \ldots \tag{14}$$

This merely says that as the mode $n$ along $\phi$ increases, the radiation due to the source decreases and eventually becomes vanishingly small as $n \to \infty$. The dominance of $p_0$ implies that the most powerful radiation comes when the ring is without any periodicity along $\phi$ direction or, equivalently, the ring

turns out to be an axisymmetric doughnut-type, which finds support in the works Crow and Champagne,[1] Wooldridge and Wooten,[2] and Hardin.[3] This decreasing character of source radiation as $n$ increases is not at all surprising if one thinks of the physical nature of the rings with high periodicity. What happens in this case is that the positive and negative parts effectively cancel each other as $n$ goes on increasing. This is evident from Fig. 4.

Thus, in what follows, only axisymmetric rings will be considered, without any periodicity along $\phi$, so that the factor involving $e^{in\phi}$ will be completely absent in all of the mathematical expressions.

To predict the intensity of radiation due to the source in the secondary stream, the fundamental solutions associated with various quadrupoles must be employed in a specific manner to represent the radiation pattern due to an axially symmetric sound field. The works of Ribner[15] and Mani[4,5] suggest that the far-field intensity due to a ring source in the cold secondary stream $I_{rcs}$ may be evaluated from the formula

$$I_{rcs} \approx \sum_{i,j=1}^{3} \langle \tilde{a}_{ij}^2 \rangle \tag{15}$$

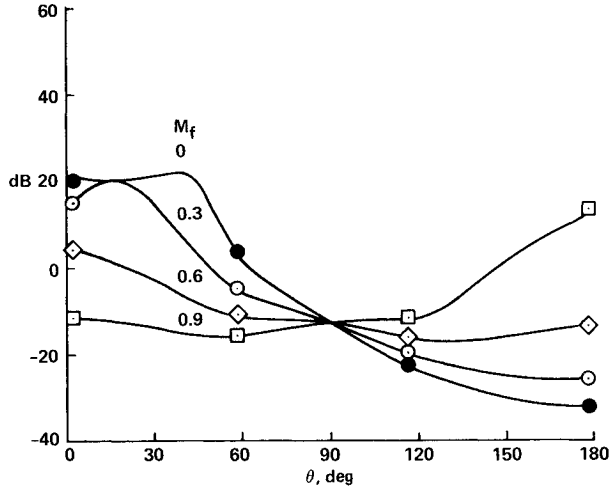


**a) Inverted velocity profile, $M_p = 0.5$, $M_s = 0.9$.**

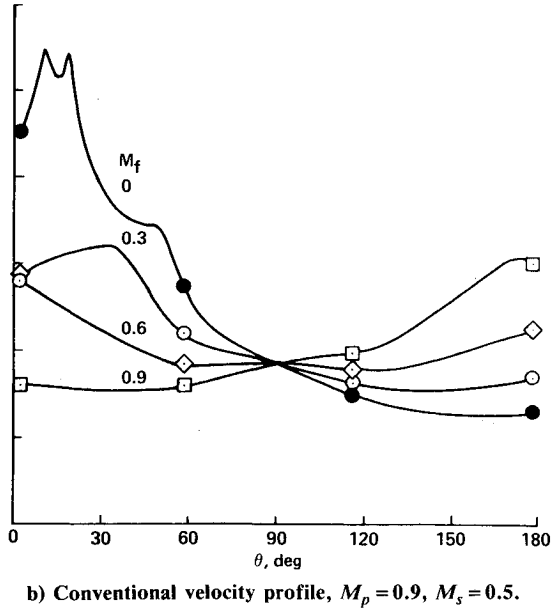


**b) Conventional velocity profile, $M_p = 0.9$, $M_s = 0.5$.**

**Fig. 5 Change in directional intensity as a result of flight at an outer-to-inner area ratio $\Sigma = 1$.**

Here $\langle \tilde{a}_{ij}^2 \rangle$ is used to represent the circumferential average of the mean square value of the enclosed quantity, where

$$\langle \tilde{a}_{ij}^2 \rangle = \frac{1}{2\pi}\int_0^{2\pi} \tilde{a}_{ij}^2 \mathrm{d}\phi, \quad \tilde{a}_{ij}^2 = (a_{ij})(a_{ij}^*) \tag{16}$$

The subscripts in these equations characterize the type of quadrupole and the asterisk implies its complex conjugate. Following the procedure outlined in these references, we have

$$a_{11} = \frac{\rho_s \mathcal{K}_s}{i\pi r_s \tau_0}\left[\frac{\mathcal{K}_s \tau_0 (C_0 - C_2)}{2}\cos^2\phi + C_1 \sin^2\phi\right]\mathrm{Exp}_1(\mathfrak{R}) \tag{17a}$$

$$a_{22} = \frac{\rho_s \mathcal{K}_s}{i\pi r_s \tau_0}\left[\frac{\mathcal{K}_s \tau_0 (C_0 - C_2)}{2}\sin^2\phi + C_1 \cos^2\phi\right]\mathrm{Exp}_1(\mathfrak{R}) \tag{17b}$$

$$a_{33} = \frac{\rho_s}{i\pi r_s}\left(k\frac{c_0}{c_f}\right)^2 \cos^2\theta \cdot C_0 \mathrm{Exp}_3(\mathfrak{R}) \tag{17c}$$

$$a_{12} = \frac{\rho_s \mathcal{K}_s}{i\pi r_s \tau_0}\sin\phi\cos\phi\left[\frac{\mathcal{K}_s \tau_0 (C_0 - C_2)}{2} - C_1\right]\mathrm{Exp}_1(\mathfrak{R}) \tag{17d}$$

$$a_{13} = \frac{\rho_s \mathcal{K}_s}{\pi r_s} k\frac{c_0}{c_f}\cos\theta\cos\phi \cdot C_1 \mathrm{Exp}_2(\mathfrak{R}) \tag{17e}$$

$$a_{23} = \frac{\rho_s \mathcal{K}_s}{\pi r_s} k\frac{c_0}{c_f}\cos\theta\sin\phi \cdot C_1 \mathrm{Exp}_2(\mathfrak{R}) \tag{17f}$$

$$C_n = \frac{J_n(\mathcal{K}_s\tau_0)\mathcal{G}_{sp}(Y_0,J_0) - Y_n(\mathcal{K}_s\tau_0)\mathcal{G}_{sp}(J_0,J_0)}{\mathcal{G}_{fs}(H_0,J_0)\mathcal{G}_{sp}(Y_0,J_0) - \mathcal{G}_{fs}(H_0,Y_0)\mathcal{G}_{sp}(J_0,J_0)} \tag{17g}$$

$$\mathrm{Exp}_n(\mathfrak{R}) = \frac{\exp i(\mathfrak{R}kc_0/c_f - wt)}{\mathfrak{R}[1 - c_0/c_f(\mathfrak{M}_c - M_f)\cos\theta]^n} \tag{17h}$$

so that

$$\begin{aligned} I_s &= \langle \tilde{a}_{33}^2 \rangle + 2\langle \tilde{a}_{11}^2 \rangle + 2\langle \tilde{a}_{12}^2 \rangle + 4\langle \tilde{a}_{13}^2 \rangle \\ &= \left(\frac{\rho_s}{\pi \mathfrak{R} r_s \tau_0}\right)^2 \frac{1}{Q_2^2 |\delta_2|^2}\left\{\frac{|\gamma_0|^2 \lambda_{3s}^2 (c_0/c_f)^4 \cos^4\theta}{Q_2^2 |M_2|^2}\right. \\ &+ \left|\frac{3}{16}[x_2(\gamma_0 - \gamma_2)]^2 + \frac{3}{4}\gamma_1^2 + \frac{x_2\gamma_1}{4}(\gamma_0 - \gamma_2)\right| \\ &+ \left|\frac{1}{16}[x_2(\gamma_0 - \gamma_2)]^2 + \frac{\gamma_1^2}{4} - \frac{x_2\gamma_1}{4}(\gamma_0 - \gamma_2)\right| \\ &\left. + \frac{2|\gamma_1|^2 \lambda_{3s}^2 (c_0/c_f)^2 \cos^2\theta}{Q_2^2}\right\} \end{aligned} \tag{18a}$$

where

$$\begin{aligned} \delta_2 &= E\beta_2 J_0(u_2) + \alpha_2 J_1(u_2) \\ \alpha_2 &= H_0(y_2) W_0(v_2, w_2) - F H_1(y_2) L_0(w_2, v_2) \\ \beta_2 &= H_0(y_2) L_1(v_2, w_2) - F H_1(y_2) W_0(w_2, v_2) \\ \gamma_0 &= -J_1(u_2) L_0(v_2, x_2) + E J_0(u_2) W_0(x_2, v_2) \\ \gamma_1 &= J_1(u_2) W_0(v_2, x_2) - E J_0(u_2) L_1(x_2, v_2) \\ \gamma_2 &= J_1(u_2) V(x_2, v_2) - E J_0(u_2) U(x_2, v_2) \end{aligned} \tag{18b}$$

$$W_0(z,\zeta) = -J_0(z)\,Y_1(\zeta) + J_1(\zeta)\,Y_0(z)$$

$$L_0(z,\zeta) = J_0(z)\,Y_0(\zeta) - J_0(\zeta)\,Y_0(z)$$

$$L_1(z,\zeta) = J_1(z)\,Y_1(\zeta) - J_1(\zeta)\,Y_1(z)$$

$$U(z,\zeta) = J_2(z)\,Y_1(\zeta) - J_1(\zeta)\,Y_2(z)$$

$$V(z,\zeta) = J_2(z)\,Y_0(\zeta) - J_0(\zeta)\,Y_2(z) \qquad (18c)$$

$$u_2 = \mathcal{K}_p r_p, \quad v_2 = \mathcal{K}_s r_p, \quad w_2 = \mathcal{K}_s r_s$$

$$x_2 = \mathcal{K}_s r_0, \quad y_2 = \mathcal{K}_f r_s, \quad z,\zeta = \text{dummary variables} \qquad (18d)$$

$$M_1 = \left[W_1 - \left(\frac{c_0}{c_f}\cos\theta\right)^2\right], \quad M_2 = \left[W_2 - \left(\frac{c_0}{c_f}\cos\theta\right)^2\right]$$

$$W_1 = \left(\frac{c_0}{c_p}\right)^2\left[1 - \frac{c_0}{c_f}(M_p - M_f)\cos\theta\right]^2$$

$$W_2 = \left(\frac{c_0}{c_s}\right)^2\left[1 - \frac{c_0}{c_f}(M_p - M_f)\cos\theta\right]^2$$

$$E = \left(\frac{M_2}{M_1}\right)\left(\frac{W_1}{W_2}\right), \qquad F = \left(\frac{W_2}{M_2}\right)\frac{c_0}{c_f}\sin\theta$$

$$Q_2 = 1 - \frac{c_0}{c_f}(\mathfrak{M}_c - M_f)\cos\theta \qquad (18e)$$

$$k_{rp} = St_2\left[\frac{\pi\bar{M}}{Q_2\Gamma^{1/2}(1+\Sigma)^{1/2}}\right]$$

$$k_{rs} = k_{rp}(1+\Sigma)^{1/2}, \qquad k r_0 = (kr_p + kr_s)/2 = \lambda_{3s}$$

$$St_2 = \left(\frac{w}{2\pi}\frac{D}{U_m}\right)\left(\frac{U_s}{U_p}\right)^{1/2} Q_2, \qquad D = 2r_s \qquad (18f)$$

$$\bar{M} = \left[\frac{M_p^2}{1+\Sigma}\frac{1}{P_1} + \frac{M_s^2\Sigma}{1+\Sigma}\frac{1}{P_2}\right]^{1/2} = \frac{U_m}{c_0}$$

$$\Gamma = \frac{U_s}{U_p}, \qquad \Sigma = \frac{\pi(r_s^2 - r_p^2)}{\pi r_p^2}$$

$$P_1 = \rho_0/\rho_p, \qquad P_2 = \rho_0/\rho_s, \qquad \rho_f \sim \rho_0 \qquad (18g)$$

The symbol $\Gamma$ represents the outer-to-inner velocity ratio and $\Sigma$ the outer-to-inner area ratio. $U_m$ is a characteristic mean velocity obtained from the conservation of momentum equation for the coaxial jet and $\bar{M}$ its corresponding Mach number defined with respect to $c_0$. $St_2$ is the source Strouhal number observed in a frame of reference convected at a Mach number $(\mathfrak{M}_c - M_f)c_0/c_f$ and is related to the observed Strouhal number by a Doppler factor $[1 - c_0/c_f \times (\mathfrak{M}_c - M_f)\cos\theta]$. This is also called the Doppler-corrected Strouhal number. This provides relative velocity between the nozzle and the observer, which is actually the case in the real situation (where the nozzle moves and the observer is static). To get the exact far-field intensity, we must now take into consideration the intensity of radiation due to the ring source in the cold primary flow. This is obtained in exactly the same way as was done for the ring source in the cold secondary stream.

## Ring Source in the Primary Stream

The noise sources arising as a result of the interaction due to the primary and secondary flows is represented by considering a ring source convecting in the midst of the primary flow at a radial distance of $r = r_0$ from the axis of the flow.

The general motion of acoustic propagation is governed by the following equations:

$$\left[\frac{1}{c_p^2}\left(\frac{\mathrm{D}}{Dt}\right)_p^2 - \nabla^2\right]p = q_m L_j\left\{\frac{\delta(r-r_0)}{r}\delta(z - U_c t)e^{i(m\phi - \omega t)}\right\}, \quad 0 \le r \le r_p \qquad (19a)$$

$$\left[\frac{1}{c_s^2}\left(\frac{\mathrm{D}}{Dt}\right)_s^2 - \nabla^2\right]p = 0, \quad r_p \le r \le r_s \qquad (19b)$$

$$\left[\frac{1}{c_f^2}\left(\frac{\mathrm{D}}{Dt}\right)_f^2 - \nabla^2\right]p = 0, \quad r_s \le r \qquad (19c)$$

The boundary conditions are given by Eq. (7) with $M_c$ replaced by $\mathfrak{M}_c$. Use of Eq. (15) and the earlier procedure yields the intensity for far-field radiation due to a ring source in the cold primary stream

$$I_{rcp} = \langle \bar{b}_{33}^2 \rangle + 2\langle \bar{b}_{11}^2 \rangle + 2\langle \bar{b}_{12}^2 \rangle + 4\langle \bar{b}_{13}^2 \rangle$$

$$= \left(\frac{2\rho_p}{\pi^2 R r_s r_p}\right)^2 \frac{1}{|M_2\delta_1|^2}\left\{\frac{(c_0/c_f)^4\cos^4\theta}{Q_1^2}\left|\frac{J_0(x_1)}{M_1}\right|^2 + \frac{1}{\lambda_{3p}^2}\left|\frac{3}{16}x_1^2[J_0(x_1) - J_2(x_1)]^2 + \frac{3}{4}[J_1(x_1)]^2 + \frac{x_1 J_1(x_1)}{4}[J_0(x_1) - J_2(x_1)]\right|^2 + \frac{1}{\lambda_{3p}^2}\left|\frac{x_1^2}{16}[J_0(x_1) - J_2(x_1)]^2 + \frac{1}{4}[J_1(x_1)]^2 - \frac{x_1 J_1(x_1)}{4}[J_0(x_1) - J_2(x_1)]\right|^2 + \frac{2(c_0/c_f)^2\cos^2\theta}{Q_1^2}|J_1(x_1)|^2\right\} \qquad (20a)$$

where $R$ is the distance between the center of the ring source and the observer's position and $\theta$ the angle made by this line with the direction of convection, all considered at the time of emission. Other quantities are defined as follows:

$$\delta_1 = E\beta_1 J_0(u_1) + \alpha_1 J_1(u_1)$$

$$\alpha_1 = H_0(y_1)W_0(v_1, w_1) - FH_1(y_1)L_0(w_1, v_1)$$

$$\beta_1 = H_0(y_1)L_1(v_1, w_1) - FH_1(y_1)W_0(w_1, v_1) \qquad (20b)$$

$$u_1 = K_p r_p, \quad v_1 = K_s r_p, \quad w_1 = K_s r_s$$

$$x_1 = K_p r_0, \quad y_1 = K_f r_s \qquad (20c)$$

$$Q_1 = 1 - (c_0/c_f)(M_c - M_f)\cos\theta \qquad (20d)$$

$$kr_p = St_1\left[\frac{\pi\bar{M}}{Q_1\Gamma^{1/2}(1+\Sigma)^{1/2}}\right]$$

$$kr_s = kr_p(1+\Sigma)^{1/2}, \quad kr_0 = kr_p/2 = \lambda_{3p} \qquad (20e)$$

$$St_1 = \left(\frac{\omega}{2\pi}\frac{D}{U_m}\right)\left(\frac{U_s}{U_p}\right)^{1/2} Q_1 \qquad (20f)$$

The propagating constants $K_p$, $K_s$, and $K_f$ are obtained from Eq. (11) by replacing the convection Mach number $\mathfrak{M}_c$ of the ring source in the secondary stream by the convection Mach number $M_c$ of the ring source in the primary stream. As before, $St_1$ is the source Strouhal number where the source is moving with a Mach number $(M_c - M_f)c_0/c_f$ in the

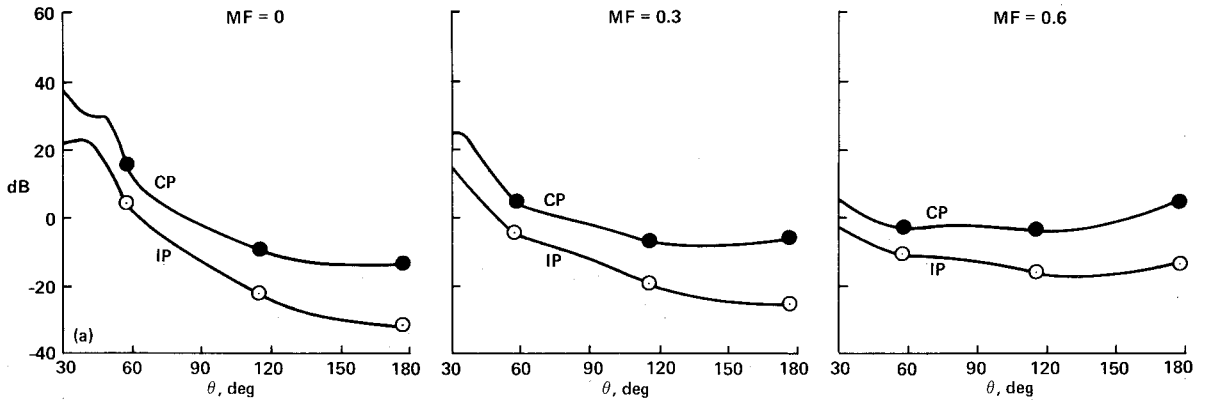


**Fig. 6a Comparison of SPL due to conventional profile (CP) and inverted profile (IP) at an equal mass flow and thrust and area ratio $\Sigma = 1$. (● CP: $M_p = 0.9$, $M_s = 0.5$, $\bar{M} = 0.73$; ⊙ IP: $M_p = 0.5$, $M_s = 0.9$, $\bar{M} = 0.73$).**

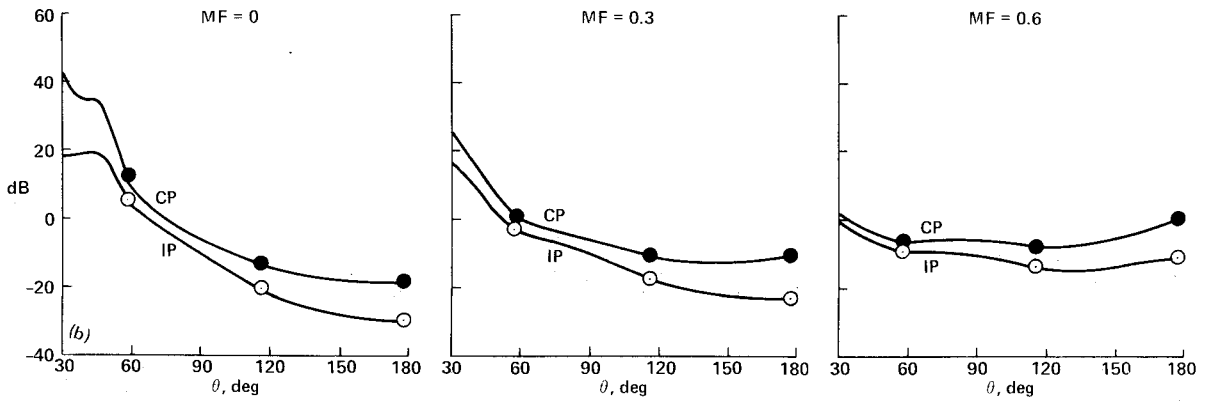


**Fig. 6b Comparison of SPL due to conventional profile (CP) and inverted profile (IP) at unequal mass flow and thrust and area ratio $\Sigma = 4$. (● CP: $M_p = 0.9$, $M_s = 0.5$, $\bar{M} = 0.60$; ⊙ IP: $M_p = 0.5$, $M_s = 0.9$, $\bar{M} = 0.84$).**

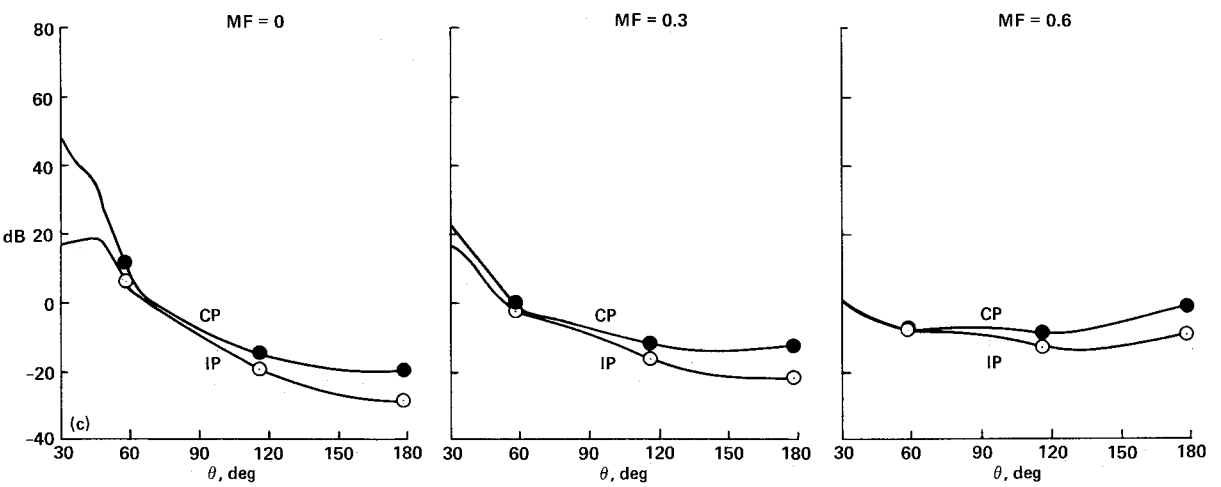


**Fig. 6c Comparison of SPL due to conventional profile (CP) and inverted profile (IP) at unequal mass flow and thrust and area ratio $\Sigma = 10$. (● CP: $M_p = 0.9$, $M_s = 0.5$, $\bar{M} = 0.55$; ⊙ IP: $M_p = 0.5$, $M_s = 0.9$, $\bar{M} = 0.87$).**

frame of reference moving with flight velocity in the simulated environment. The notation $I_{rcp}$ in Eq. (20) is introduced to signify that it implies the intensity due to radiation from a ring source in the cold primary stream.

## Intensity of Radiation due to Both Ring Sources in Cold Coaxial Flow and Application of the Theory

Since the problem under consideration is a linear one, the effective radiation due to the coaxial dual flow phenomenon will be considered as the linear combination of the two radiation fields generated by the ring sources in the primary flow and secondary flow. Consequently, the intensity of radiation in the far field is given as the combined effects of the intensities given in Eqs. (18) and (20). This is expressed as

$$I = \left(\frac{\rho_f}{R}\right)^2 \frac{64(1+\Sigma)}{\pi^4 D^4} \left[\frac{RCP}{P_1^2} + \left(\frac{\pi}{1+\sqrt{1+\Sigma}}\right)^2 \frac{PCS}{P_2^2}\right] \quad (21a)$$

where $D$ is the external diameter of the coaxial jet [and is related to the internal diameter through the relation

$D = d(1+\Sigma)^{1/2}$] and

$$RCP = I_{rcp}\left(\frac{\pi^2 R r_s r_p}{2\rho_p}\right)^2 \tag{21b}$$

$$RCS = I_{rcs}\left(\frac{\pi R r_s \tau_0}{\rho_s}\right)^2 \tag{21c}$$

To make a straightforward linear combination of the radiation effects and also to keep the involved mathematics less complicating, we have considered a situation where the centers of the ring sources coincide and as such their radiations reach the observer simultaneously. In such a situation, $R = \mathfrak{R}$ and $\theta$, the angle of emission at the retarded time, is the same for both. This fact has been accounted for in developing the expression for the intensity of radiation due to both rings as given in Eq. (21).

In all the plots, the computation is made for the directional intensity at Strouhal numbers $St_1 = 0.2$ and $St_2 = 0.2$, and is expressed in terms of sound pressure levels (in decibels) where

$$\text{dB} = 10 \log_{10} I(M_f) \tag{22a}$$

$$I(M_f) = \frac{64}{\pi^4}(1+\Sigma)\left[\frac{RCP}{P_1^2} + \left(\frac{\pi}{1+\sqrt{1+\Sigma}}\right)^2 \frac{RCS}{P_2^2}\right] \tag{22b}$$

The parameter values of $P_1 = 1 = P_2$ implies the consideration of a cold coaxial jet where $\rho_p = \rho_s = \rho_f$. Furthermore, while making computations, the convection Mach number of the ring source in the primary flow is given by $M_c = (M_p + M_s)/2$ and the convection Mach number of the ring source in the secondary flow is given by $\mathfrak{M}_c = (M_s + M_f)/2$. This form of the convection Mach numbers is used to reflect the speeds of the flows whose interactions are solely responsible for the generation of these sources.

With these assumptions, the directivity pattern of intensity level is shown in Figs. 5 and 6 for two representative ring sources. Figure 5a represents a coaxial flow situation where the inner/primary flow Mach number ($M_p = 0.5$) is lower than the outer/secondary flow Mach number ($M_s = 0.9$) and represents an inverted velocity profile configuration. Figure 5b represents an altogether different flow profile where the primary and secondary flows are completely inverted. This coaxial flow pattern is called the conventional velocity profile configuration. In both figures, one notices that as we move from a static ($M_f = 0$) to flight situation ($M_f > 0$), the intensity of radiation in the aft quadrant ($0 \le \theta \le \pi/2$) diminishes and the intensity of radiation in the forward quadrant ($\pi/2 \le \theta \le \pi$) increases. In other words, forward speed induces amplification of noise in the forward quadrant and reduction of noise in the aft quadrant. Another point of interest is the crossing of all the curves at $\theta = 90$ deg. Their coalescence at one point implies that at $\theta = 90$ deg, the impact or the effects of flight are completely absent.

In both these figures, it can be seen that the inversion of velocities, from high-inner/low-outer to low-inner/high-outer, causes a substantial reduction in the radiation at all angles. Thus, under constant thrust and mass flow conditions, an inverted velocity profile coaxial jet is quieter than a conventional velocity profile coaxial jet. This point is more explicitly illustrated in Figs. 6a-6c, which reassert the fact that an inverted velocity profile retains its quieting quality not only when there is no flight, but also at practically all flight conditions.

In Fig. 6a the comparison of SPL from the conventional velocity profile jet and the inverted velocity profile jet is made at constant mass flow and constant thrust, at area ratio $\Sigma = 1$. The noise reduction due to the inverted profile jet relative to the conventional profile jet is at least 10 dB in the aft quadrant and around 16 dB in the forward quadrant. In going from the static to the flight case, the static benefit in noise reduction in the aft quadrant is diminished by nearly 1.5 dB at $M_f = 0.3$ and by 2 dB at $M_f = 0.6$, whereas that in the forward quadrant is more or less maintained. Nonetheless, as a result of flight, the overall SPL in the aft quadrant is reduced and that in the forward quadrant is enhanced. This observation is in tune with our earlier findings[10-12] where we noted that the effects of flight induce reduction of noise in the aft quadrant and amplification of noise in the forward quadrant.

When the area ratio is increased to $\Sigma = 4$ and 10 as in Figs. 6b and 6c, respectively, the inverted velocity profile jet provides higher bypass ratios and increased mass flow and increased thrust. This is not the case for the conventional profiles when the mass flow and thrust are substantially reduced as a result of the increasing area ratio. Comparison of all the plots of Fig. 6 indicates that the attenuation obtained over all angles as a result of flow inversion is substantial when a low area ratio (and hence a low-bypass-ratio operation) is maintained. It is worthwhile to give an explanation on the physical mechanisms for the predicted lower noise of the inverted velocity profile coaxial jets as compared to the conventional profile coaxial jets. One of the most important factors in the inherently low noise of inverted velocity profile jets is that the higher-velocity region has a small characteristic dimension so that the most intense noise-generating region is limited to a small volume. Furthermore, because of the inverted profile distribution of acoustic impedance, a significant fraction of the noise generated is trapped within the jet and does not radiate to the far field.

## Conclusions

The effects of flight on coaxial jet noise have been studied on the basis of a double-vortex sheet flow model. The elegance of handling the problem comes through the deliberate suppression of the flow instabilities and also through the inherent simplicity of the vortex sheet model. The conclusions of investigation are based on the specific assumptions and calculations introduced in our model. Accordingly, as a result of this study, we find that the effects of flight on noise from an unheated coaxial dual flow induce:

1) Amplification of noise in the forward quadrant ($\pi/2 \le \theta \le \pi$).

2) Reduction of noise in the aft quadrant ($0 \le \theta \le \pi/2$).

3) Absolutely no impact on noise at $\theta = 90$ deg to the jet axis.

Furthermore, the results of this study indicate that:

4) At constant mass flow and thrust maintained at an outer-to-inner area ratio $\Sigma$ equal to unity, an inverted velocity profile jet is at least 10 dB (SPL) quieter than a conventional profile jet at all angles in the aft quadrant and 16 dB (SPL) quieter at all angles in the forward quadrant when there is no flight.

5) The static benefit in noise reduction is more or less maintained in the forward quadrant, but is somewhat lost by nearly 1.5-2 dB in the aft quadrant.

6) The amount of noise reduction due to an inverted velocity profile jet (relative to a conventional profile jet) gradually diminishes as the area ratio $\Sigma$ increases.

## Acknowledgments

This study was conducted as part of a NASA Ames program of research into flight effects on jet noise under NASA Cooperative Agreement Contract NCC 2-75. I am thankful to David H. Hickey and Adolph Atencio Jr. of NASA Ames, and K. Karamcheti of Stanford for the benefit of discussion and to Yen Liu of Stanford for his immense help in programming these calculations. I am most deeply indebted to J. R. Stone of NASA Lewis for his ideas, which have helped me in giving an explanation for the predicted lower noise of the inverted profile coaxial flows. My thanks

are also due to H. K. Tanna of Lockheed-Advanced Aeronautics and Warren F. Ahtye of NASA Ames for their useful suggestions and comments, which have helped the author to present the paper in the above form.

## References

[1]Crow, S. C. and Champagne, F. H., "Orderly Structures in Jet Turbulence," *Journal of Fluid Mechanics*, Vol. 48, Pt. 3, 1971, pp. 547-591.

[2]Wooldridge, C. E. and Wooten, D. C., "A Study of the Large-Scale Eddies of Jet Turbulence Producing Jet Noise," AIAA Paper 71-154, 1971.

[3]Hardin, J. C., "Noise Produced by the Large-Scale Transition Region Structure of Turbulent Jets," AIAA Paper 74-550, 1974.

[4]Mani, R., "The Influence of Jet Flow on Jet Noise, Part I: The Noise of Unheated Jets," *Journal of Fluid Mechanics*, Vol. 73, Pt. 4, 1976, pp. 753-778.

[5]Mani, R., "The Influence of Jet Flow on Jet Noise, Part 2: The Noise of Heated Jets," *Journal of Fluid Mechanics*, Vol. 73, Pt. 4, 1976, pp. 779-793.

[6]Phillips, O. M., "On the Generation of Sound by Supersonic Turbulent Shear Layers," *Journal of Fluid Mechanics*, Vol. 9, Pt. 1, 1960, pp. 1-28.

[7]Lilley, G. M., "The Generation and Radiation of Supersonic Jet Noise," AFAPL-TR-72-53 Vol. IV, 1972.

[8]Goldstein, M. E. and Howes, W. L., "New Aspects of Subsonic Aerodynamic Noise Theory," NASA TN D-7158, 1973.

[9]Balsa, T. F. and Gliebe, P. R., "Aerodynamics and Noise of Coaxial Jets," *AIAA Journal*, Vol. 15, Nov. 1977, pp. 1550-1558.

[10]Dash, R., "Analysis of Flight Effects on Noise Radiation from Jet Flow Using a Convecting Quadrupole Model," AIAA Paper 78-192, 1978.

[11]Dash, R., "Analysis of Flight Effects on Noise Radiation from Dual-Flow Coaxial Jets," AIAA Paper 79-0619, 1979.

[12]Dash, R., "Effects of Forward Velocity on Sound Radiation from Convecting Monopole and Dipole Sources in Jet FLow," *Journal of Sound and Vibration*, Vol. 64 (2), 1979, pp. 187-207.

[13]Scharton, T. D., White, P. H., and Rentz, P. E., "Supersonic Jet Noise Investigation Using Jet Fluctuating Pressure Probes," Bolt Beranek and Newman Inc., Cambridge, MA, Rept. 2220, 1973.

[14]Mani, R., "Further Studies on Moving Source Solutions Relevant to Jet Noise," *Journal of Sound and Vibration*, Vol. 35 (1), 1974, pp. 101-117.

[15]Ribner, H. S., "Quadrupole Correlations Governing the Pattern of Jet Noise," *Journal of Fluid Mechanics*, Vol. 38, Pt. 1, 1969, pp. 1-24.

[16]Dash, R., "Flight Effects on Noise from Coaxial Dual Flow, Part II: Heated Jets," *AIAA Journal*, to be published.